Progress in Oceanography 206 (2022) 102840

Contents lists available at ScienceDirect

Progress in Oceanography

journal homepage: www.elsevier.com/locate/pocean

The 2015 exceptional swell in the Southern Pacific: Generation, advection, forecast and implied extremes

L. Cavaleri [a,*], A. Benetazzo [a], L. Bertotti [a], J.-R. Bidlot [b], A. Pomaro [a], J. Portilla-Yandun [c]

[a] Institute of Marine Sciences, Venice, Italy
[b] European Centre for Medium-Range Weather Forecasts, Reading, UK
[c] Research Center of Mathematical Modelling (MODEMAT), Escuela Politecnica National, Quito, Ecuador

ARTICLE INFO

Keywords:
Antarctic storms
Wave modelling
Pacific swell
Energy advection
Swell wave and max wave heights
Extremely low-frequency forerunners

ABSTRACT

A very severe storm in the Antarctic belt is analysed that sent a very large swell throughout the South-Pacific Ocean. The reasons for the storm were a deep depression passing over an anomalous warm sea area, with consequent increased intensity, more active wind input, gustiness, with also dynamical generation. Wind and wave model results are verified with scatterometer and altimeter data. We follow the swell evolution during the five days required to reach the Galapagos Islands and a buoy off the Peruvian coast. The first forerunners peaked at 0.032 Hz at these locations, well represented in the model thanks to a purposely extended frequency range used in the WAM model. A nonlinear combined analysis is carried out to estimate the overall maximum single wave heights that may have impinged on the Galapagos coasts. Single wave heights up to 6 m have been estimated. Once generated, the swell conditions at Galapagos and the buoy are perfectly anticipated. Including generation, useful forecasts extend till at least eight days before the event. The lack of any local communication is discussed. An analysis using ERA5 winds, but a respectively higher resolution long-term wave hindcast, shows that a similar, actually stronger, event happened in 2006. A simple, but sound method, based on physical principles and elementary geometry, is proposed to estimate, firsthand and after any time, the maximum height of a once generated swell. The results for the 2015 storm are correct within 5% of the model values.

Acronyms and symbols

ECMWF	European Centre for Medium-Range Weather Forecasts
WHOI	Woods Hole Oceanographic Institute
NOAA-NCEP	National Oceanic and Atmospheric Administration – National Center for Environmental Prediction
WAM	WAve Model
ecWAM	the WAM version run at ECMWF
ERA5	ECMWF ReAnalysis
JONSWAP	Joint North Sea Wave Project
H_s	significant wave height
H_{max}	maximum wave height in a record or time period
T_m	mean wave period
T_p	peak period

1. The event and its analysis

In late April to early May 2015, an unusually strong Antarctic storm generated very large and long waves that spread in the South-East Pacific, sending large waves towards the South-American coast and flooding, among other places, the Galapagos Islands, 6000 km away. The event was remarkable not only for its energetic content, but also for the very low frequencies that characterized, e.g. at the islands, the local preliminary and then main waves. In this paper, after a general description of the generation event, we focus on how the large swell propagated up to the equatorial zone. We also quantify the largest wave heights which impacted the Galapagos (Islands, henceforth not repeated). We stress that our present aim is not "to tune" the models to achieve however the best possible results. Granted that improvements are always possible, different areas and situations could offer better alternatives. Conversely, given that wave models nowadays are very reliable tools, we use them to explore the generation and evolution of particular storms to better understand their nature and what to expect.

On this basis, in Section 2 we briefly characterize the Antarctic belt and the typical swell generated by the repeated local storms towards the South-East Pacific Ocean. We also summarize the model data used for

* Corresponding author.
E-mail address: luigi.cavaleri@ismar.cnr.it (L. Cavaleri).

https://doi.org/10.1016/j.pocean.2022.102840
Received 1 June 2021; Received in revised form 3 December 2021; Accepted 7 June 2022
Available online 16 June 2022

our analysis and some specific modelling carried out for the purpose. Besides, we briefly mention the available measured data used for model validation and to gain insight into the wind and wave situation. The storm is described in detail in Section 3, highlighting the estimated generation zone of the swell. Comparison with altimeter and scatterometer data provides a well-defined estimate of the (wind and waves) modelling accuracy. How the swell evolved and propagated towards the North-East is dealt with in detail in Section 4. Beside the many successive altimeter passes that offered a clear view of the progressive accuracy, we also benefitted from the data provided by the only local source of information, the WHOI-32012 buoy located at 19.4°S, 85.1°W, about 1500 km off the Peruvian coast. In Section 5, we go into detail showing how the swell conditions at Galapagos and at the buoy evolved in time. In particular, for the Galapagos, we show how, apart from model forecasts, a careful analysis of the early local wave conditions would have shown that a large swell event was about to come. The forecast aspect of the event is dealt with in Section 6, where we show two different ranges of useful forecast, respectively after and before the actual Antarctic storm. The practical consequences for Galapagos are the main subject of the following Section 7. Here, on the basis of practical, though theoretically sound, approaches, we provide an estimate of the maximum single wave heights that are expected to have affected the Galapagos coasts. We conclude our research in Section 8 with a generalized estimate of the propagation of a swell moving North from the southern storm belt, defining the affected area and the implied energy levels. The approach and the related formulas are briefly described in the Appendix A. In the final Discussion and Conclusions (Section 9), we suggest a possible reason for this particularly strong event in the Antarctic belt. From the practical point of view, we stress the need for the Galapagos users and authorities (but the statement is obviously of general significance) to use the openly available wave forecasts and information for a useful local warning. This stimulated us to explore the past to see how exceptional the 2015 event had been. Interestingly, a higher energy swell case had been present nine years earlier, in 2006. The paper is closed with a Summary (Section 10) which provides all the main findings in an itemized compact, though clear, form. A list of acronyms and symbols is given.

2. The Pacific Antarctic belt and its modelling

The Antarctic belt (see Sokolov and Rintoul, 2009, and the more recent Rintoul et al., 2018 for a full description) is characterized by a continuous West to East violent atmospheric flow around Antarctica. Ocean currents and wave fields follow accordingly. The clockwise rotation of the many atmospheric low-pressure zones keeps sending large waves towards the East, with also a strong northward component, leading to the southern swell that characterizes the South Pacific Ocean (Portilla-Yandún et al., 2020).

Global meteorological and ocean (current and wave) models reproduce the situation well, helped by the many scatterometer and altimeter data that document continuously the local situation[1]. For our present purposes, we have used the ECMWF model data. ECMWF is presently running the Tco1279 version of their IFS forecasting system (9 km resolution for the atmospheric model, 14 km for the wave one). However, in 2015 (the time of the mentioned swell), the atmospheric model was TL1279 (16 km resolution). The practical problem is that analysis data are archived at 6-hour interval, which is not suitable for the intercomparison with satellite data. Therefore, after a necessary check, we have resorted to using ERA5 reanalysis data (see Hersbach et al., 2020, for a full description) available at hourly intervals. The ERA5 meteorological model was run at 31 km resolution. While suitable for most of the surface wind fields, such a resolution may lead to an underestimate of the wind speeds in areas with strong pressure gradients, particularly with curved isobars. In addition to the check with scatterometer data, we have also cross-checked these results with the best available, i.e. TL1279.

However, this was not entirely sufficient for all our purposes. The ecWAM wave model run at ECMWF (see ECMWF, 2020 for a full description) uses 36 frequencies in geometrical progression, covering the 0.03452 –0.97017 Hz range, but the waves produced by the 2015 storm had characteristic frequencies below that range. To be sure to consider also these frequency components, we ran again the latest CY47R1 version of ecWAM (ECMWF, 2020), forced with ERA5 winds using a 22 km resolution wave grid and adding a further low frequency at 0.03138 Hz.

Extensive validation has been done using the available scatterometer and altimeter data. ASCAT-B wind fields and CryoSat-2 data have been used. As briefly mentioned in Section1, locally measured data are available from the WHOI-32012 buoy located well offshore the Peruvian coast. 1D and 2D spectra are available. We have used both the related integral quantities (wave heights and periods) and the 1D spectra.

3. The storm and its modelling

The storm (henceforth our official definition of the event) developed in the early Antarctic winter. The period of interest starts on April 25, 2015 (earliest evidence of the considered storm) to May 02, when the large swell reached the Galapagos. The relevant stormy period is documented in Fig. 2 (see Fig. 1 for its overall location). Panels a, b, and c show the evolution at 24-hour intervals, starting from April 26, 00 UTC (henceforth, we omit the year, 2015, and, when obvious, also the month). On the 26th, the storm was already well developed, with wind speeds up to 30 ms^{-1}. The storm grew larger during the following 24 h, reaching its peak at about 27 00 UTC, while moving steadily eastwards. The peak conditions are more evident in the wave (right) panels d, e, f for the same times. The almost 17 m significant wave heights H_s in panel e, 27 00 UTC, are an evident feature. One relevant detail is the speed of the storm. Checking the peak positions at 24-hour intervals, we find that the storm was moving at about 55 km h^{-1}. We will come back later to this point when discussing the local generation.

We focus here on panel 2e, which illustrates the cited peak of the wave conditions. The most intense area of the storm is shown in Fig. 3 (see Fig. 1 for its geographical position). As a result of the combination between the West to East local motion of the storm and the clockwise rotating winds, waves have different mean directions at different positions. For our present purposes, we summarize this by showing the mean wave direction at points A, B, C (see arrows) and the corresponding 2D spectra in the other panels. Note that the spectra are shown only for the 0°-150° flow direction (clockwise with respect to North). At position A (52°S, 132°W), the main flow is to 60°, i.e. towards the Chilean coast. B (52°S, 144°W) represents the area where the swell to North-East (main direction 30°-40°) was generated. At C (62°S, 145°W), we are again into the main Antarctic belt flow, with waves flowing mainly eastwards. We conclude that the waves due to reach the Galapagos a few days later were generated in the north-west sector of the storm (point B).

Having given a general picture of the storm, we need to validate the model results. We begin with an ASCAT-B scatterometer pass (see Fig. 4, and Fig. 1 for its position). Panels a and b show (a) the model wind field at 19 UTC of the 26th, and (b) the scatterometer measured section (8 min earlier). The direct comparison (model data interpolated at scatterometer positions) is in panel c. The results are summarized in Table 1. We find a 5% underestimate by the ERA5 model, more evident in the upper values range. Bias is −0.9 ms^{-1} out of the 20 ms^{-1} average. Panel d provides a more general view of the situation, merging all the data from ten different passes. In this case the underestimate is reduced to 2%

[1] The interested reader can find all the related statistics of the European Centre for Medium-Range Weather Forecasts (henceforth ECMWF, Reading, U. K. and Bonn, Germany) at https://www.ecmwf.int/en/forecasts/charts, and of the NOAA-National Center for Environmental Prediction (NCEP, Maryland, USA) at https://polar.ncep.noaa.gov/nwps/.

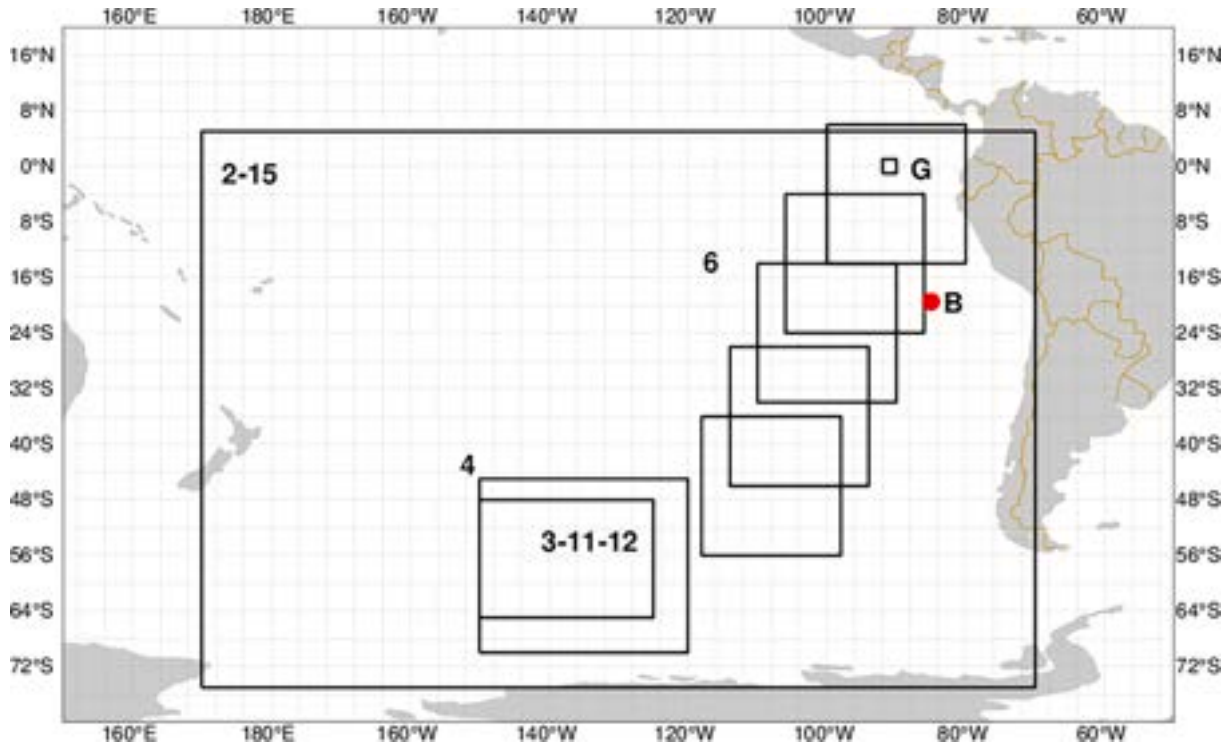

Fig. 1. The South Pacific Ocean. The numbered rectangles identify the area covered in the numbered figures. B is the buoy position. G are the Galapagos Islands.

with -0.4 ms^{-1} bias out of 15 ms^{-1} mean value. This suggests that the model tends to underestimate (at least in this storm) more the higher values, as also derived from the distribution of panel d.

On this basis, we turn our attention to the wave fields. Still close to the peak of the storm, at 20 h on the 26th, we had a useful pass by the CryoSat-2 altimeter that we indicate in Fig. 5 (note the large scale of the map, from New Zealand to South America). The ground track, black line in panel a, crosses the peak of the storm. The significant wave height (H_s) comparison is in panel b. The vertical line, corresponding to the white one in panel a (latitude 50°S), limits the area considered for the scatter plot in panel c. The fit is good, with a slight underestimate only in the southern part of the storm. See Table 1 for the overall figures. The best-fit slope (panel c) is 0.97. The overall comparison for ten useful passes (panel d) is slightly more negative (5% underestimate), but with a similar bias (~-0.4 m H_s). We stress that all these comparisons are with ERA5 wind and wave derived values.

Till now we have framed the structure of the storm and provided an idea of how well the models reproduce it. Before moving to the advection phase, it is worthwhile to argue about the possible reasons for this particularly intense storm. From the meteorological point of view, a relevant factor (see, among others, Bogen et al., 2011, and Abdalla and Cavaleri, 2002) is the air-sea temperature difference. The warmer the water, the more heat, hence energy, is transferred to the overlying atmospheric system. At the same time, the temperature difference implies a higher instability in the lowest atmospheric layers, resulting in an enhanced gustiness. The analysis of the sea temperature distribution (see Blunden and Arndt, 2016) has made evident a distribution of warmer water more to the North of the usual Antarctic belt storms position. A larger storm could easily reach this area (see Figure 3.1 at page 64 of the cited reference) and be then forced to unusually high energy levels.

Granted the higher wind speeds, the other crucial factors concern waves. With peak wind speeds close to 30 ms^{-1}, a 26–28 ms^{-1} average in the peak zone is a reasonable guess. Fully developed conditions (see Pierson and Moskowitz, 1964) for this wind speed range would be estimated at about $H_s = 2.2 * (U_{10}/10)^2 = 15$–17 m. This would require an area of a few thousand kilometres with steady high wind conditions for a couple of days at least. This appears (to be) unlikely, and therefore it suggests other factors may have been at play.

The first one is the cited gustiness that Abdalla and Cavaleri (2002) showed as crucial in enhancing wave growth for a given average wind speed. The second factor is the translational speed of the storm. The analysis of the sequential meteorological maps suggests an average motion of the meteorological system between 50 and 55 km h^{-1}, which corresponds to the group speed of 18–20 s waves, that indeed can be recognized as present, actually dominant in the spectra (panel b) of Fig. 3. If this were the case, it would imply that waves were dynamically generated, i.e., that the storm and the waves were moving together with similar speeds. Therefore, the highest winds were steadily acting on the area of the highest waves area, further enhancing their growth.

Having described the generation phase of the storm, it is now time to follow the waves in their motion to the North. This is the subject of the next section.

4. The advection phase of the storm

After April 27, the northbound swell was completely out of the generation area and now directed towards different sections of the South-American coastline, including the Galapagos, and there is no doubt that very large waves were also propagating towards the southernmost coast of Chile. We focus our attention on the northbound swell. Fig. 6 depicts well how the swell evolved along the way. Each panel (a – e) shows different areas at 24-hour intervals. Fig. 1 clarifies the different positions following the swell on its motion towards the Galapagos. Days go from April 28 to May 02. Several details deserve our attention. First, the significant wave height decreases progressively over time. This is due both to the lateral spreading of the original energy and to the different group speed of the spectral components. With the bulk of energy (see Fig. 3) between 22 and 17 s, there is a ~ 25% difference in group speed. After four days, this implies a 24-hour difference in the arrival at a certain location.

Each panel covers about 20° in latitude (see also Fig. 1). The thin line in the panels is aligned with the mean wave direction. Note the changing

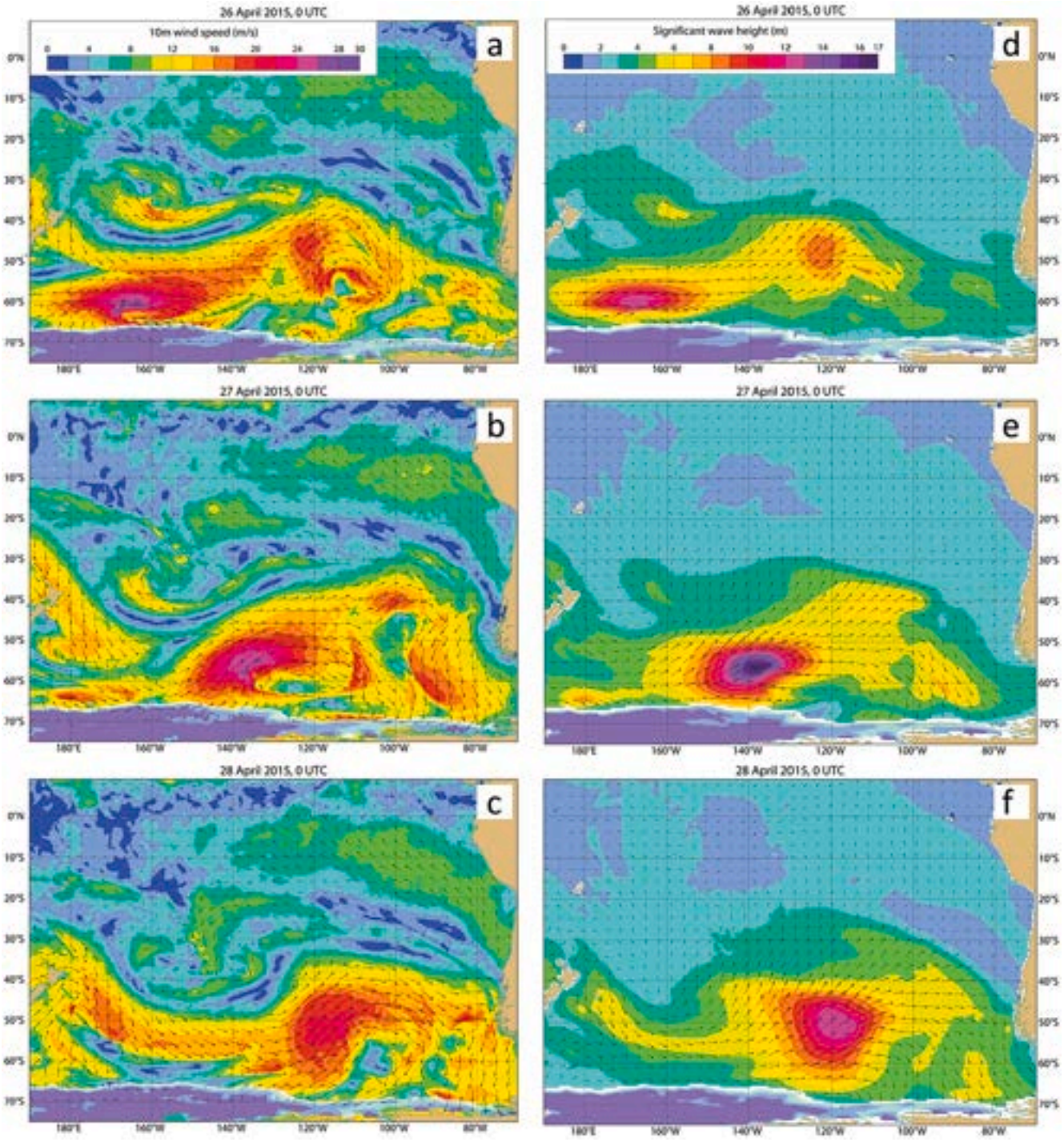

Fig. 2. South Pacific Ocean. See Fig. 1 for its geographical position. Wind (left) and wave (right) conditions at 24-hour intervals: 00 UTC of 26, 27, 28 April 2015. ERA-5 data.

mean direction from day to day. This is due to the advection along a great circle path moving from a very southern latitude towards the equator. The five corresponding H_s profiles are in the final elongated panel. Note how the swell started with a substantial 9 m peak value and it progressively decreased with the aforementioned spatial spreading of the swell overall energy. The last panel deserves a little extra explanation. As seen in Fig. 1 and in panel e, the swell reaches the Galapagos, whose shadowing is clearly visible both in panel e and in the corresponding profile of the last panel. The decrease in H_s when reaching the islands is not abrupt because the archipelago is widely scattered. Therefore, the shadowing builds up progressively while advancing among the islands. Note also the gradual catch-up of H_s after the islands, when, still within the limits of the narrowly directed swell, energy enters the shadow zone from the sides.

As done for the generation phase, we use CryoSat-2 altimeter data to validate the model values of swell. An example is provided in Fig. 7, panel a for the pass, b for the two H_s profiles, and c for the scatter diagram. The comparison is limited up to the respectively horizontal (white, panel a) and vertical (black, panel b) lines at 20°S. Table 2 summarizes the results. The fit is good, with a very limited underestimation, except for one altimeter peak value, visible as the highest value in b, corresponding to the locally enhanced H_s in a. Of course, this

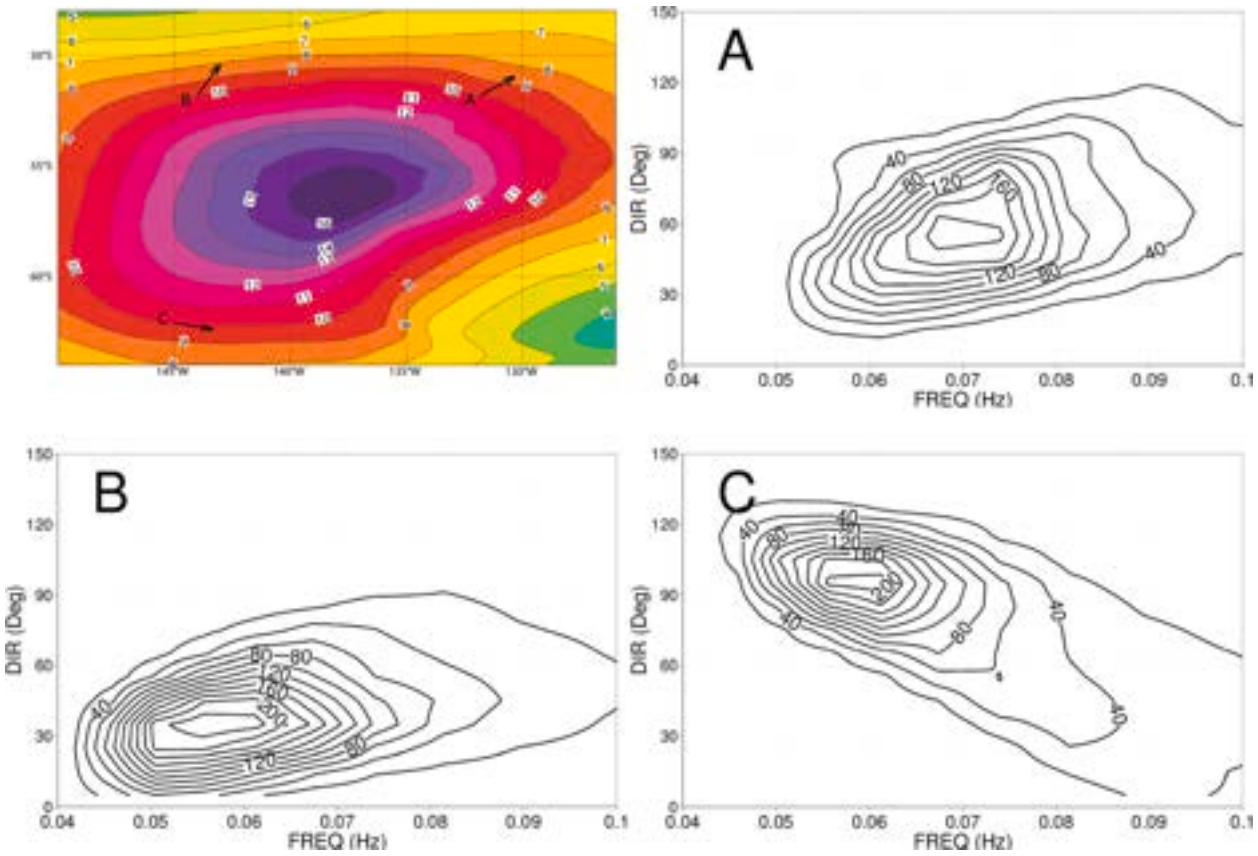

Fig. 3. The most intense phase of the storm, with the highest significant wave height. See panel 2e and Fig. 1 for the precise geographical area. Time is 27 April, 00 UTC. Isolines at 1 m interval. The wave situation at the three points A, B, C is fully provided by the 2D spectra in the respective panels (flow direction).

corresponds to the values on the far right-hand side of the two scatter plots. Panel d summarizes the comparison for ten passes. We will come back to this feature in the final discussion in Section 9.

To better frame these ERA5 results before proceeding further, we make an extensive comparison between the wave heights derived using the ERA5 (31 km resolution for the atmospheric model) and the TL1279 (16 km resolution) wind fields, respectively. The results are in Fig. 8, with panel a for the stormy area and period (26–28 April), and panel b for the swell phase (29 April- 02 May). The overall results are shown in Table 3. As expected, the ERA5 data appear slightly (3%) lower during the storm, with an evident higher underestimate for the largest H_s. Mutatis mutandis, these differences are similar to the ones visible in Figs. 4 and 5. This suggests that the TL1279 data for both wind and waves represent the marine truth at a satisfactory level. The ERA5/TL1279 comparison is better during the swell phase (panel 8b, best-fit slope 0.99), though still with an indication of some differences for the highest (greater than 8 m) H_s values. On this basis, we proceed by analysing the time evolution at the WHOI buoy and Galapagos. This is the subject of the next section.

5. The evolution of swell at Galapagos and at the buoy

As the only location where we have continuous measured data, the buoy offers a good reference to judge the performance of the models in detail. An extended comparison is offered in Fig. 9. In panel a, we show the buoy-model data for the significant wave height H_s, mean and peak periods T_m, T_p from April 29 till May 04. As expected, the continuous, smooth lines show the model results, whereas the highly variable ones are the buoy data. We will come back later to this characteristic.

Apart from missing a first H_s peak on the 30th of April, the wave height is well reproduced overall (see the statistics in Table 4), but an underestimate (~0.5 m) of the H_s peak value is evident. T_m and T_p are well reproduced throughout the event. Model and buoy directions are fully consistent. They do not convey any particular information and they are not discussed further. Note the sudden and drastic increase of the peak period on the 1st May, corresponding to the arrival of the swell forerunners (more later). The macroscopic feature is the very large variability of the measured integral quantities, a fact we deal more with in the Discussion and Conclusions of Section 9.

The differences between model and measured data at the peak of the swell are even more apparent when comparing the model and measured spectra. This is displayed in panel 9b, where we represent four stages of the swell evolution in time; buoy continuous lines, model dashed ones. Specific dates and times are indicated in the figure. During the general background of the swell (April 30), the spectra are very similar, both showing a slight peak at 25 sec period. The latter becomes macroscopic ten hours later, with the arrival of the first large swell. The model spectrum is obviously too low. This is more the case at the peak of the local conditions (15 UTC on 1th May), when the model peak energy value is about half of the measured one. Ten hours later conditions are much reduced, with a better fit of the two spectra.

All this suggests that there were indeed a few hours with very heavy conditions, both at the buoy and, about one day later, at the facing Peruvian coast. On this basis, we analyse how the situation evolved at the Galapagos. This is shown in Fig. 10 where, to better highlight the role of the forerunners, we use a logarithmic scale for the spectral density. Note that, given their different positions (see Fig. 1) in the ocean, there was almost a two days difference between the heavy conditions at the two locations. In Fig. 10, the spectra are shown at 12-hour intervals. On May 01, 00 UTC there is the expected background swell, with the peak at 0.06 Hz. However, a keen eye spots the “anomalous” peak between 0.03 and 0.04 Hz. It is worth remembering that this was

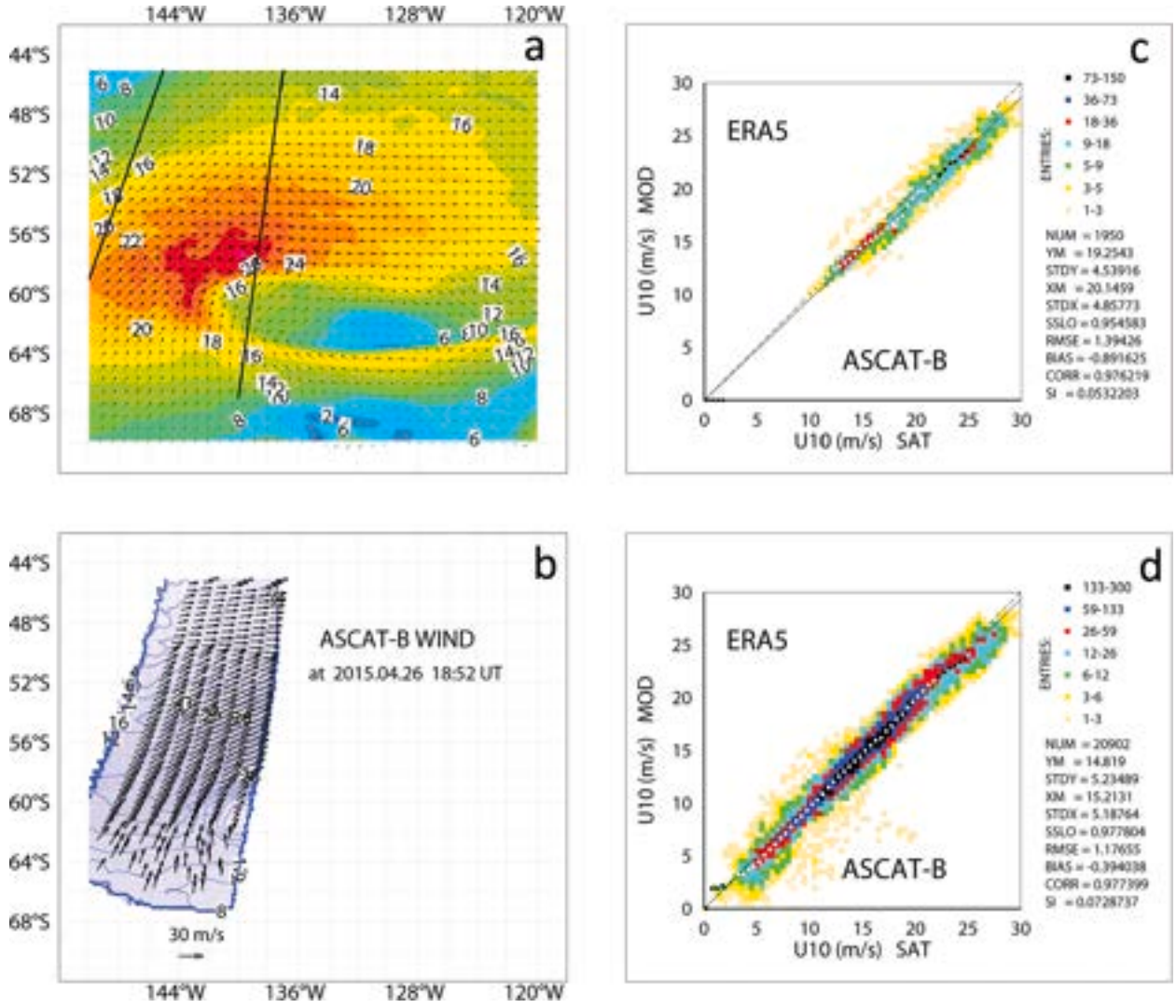

Fig. 4. Comparison between ERA5 wind fields and ASCAT-B scatterometer data. Panels a, b show one pass whose comparison results are in panel c. Panel d summarizes the statistics out of ten passes during the generation phase of the storm. The statistics are reported in Table 1.

Table 1
With reference to Figs. 4 and 5, statistics of the comparison between model values versus ASCAT-B scatterometer (wind speed) and CryoSat-2 altimeter (wave height) data. Dates are 25–26 April 2015. The focus is on the generation area. corr = correlation, SI scatter index, sslo symmetric slope.

wind speed	$\bar{U}_{10}$ (ms^{-1})	bias (ms^{-1})	corr	SI (%)	sslo
1 pass	20.15	−0.89	0.98	5.3	0.95
10 passes	15.21	−0.39	0.98	7.8	0.98
sig. wave height	$\bar{H}_s$ (m)	bias (m)	corr	SI (%)	sslo
1 pass	10.48	−0.41	0.97	7.8	0.97
10 passes	7.46	−0.37	0.97	9.7	0.95

only possible because the ecWAM model was run with an extra low frequency (0.03138 Hz). After about 12 h, this low-frequency peak is ten times larger, with a period of about 24 s. Note that this very low frequency energy corresponds to about 0.5 m swell. As time passes, both energy and frequency grow with the arrival of the main swell system. The hourly model (ERA5) data suggest that the peak conditions of 3.15 m H_s were on May 2, at 15 UTC, with only centimetric differences between the immediately preceding and following hours. The conditions at the Galapagos were very heavy for a while, with high and long, hence powerful, waves impinging on the coast. We go deeper into this aspect in Section 7. Note that the geological origin of the islands (see, e.g. Harpp and White, 2001) implies deep water conditions, practically up to the coasts, hence the extended damage of the coastal structures. It is of course of interest to see if any warning would have been possible, so we explore this next by analysing the forecast of the storm.

6. The forecast

High-resolution model forecasts are regularly available from the major meteorological centres up to 10–15 days ahead and further. While a proper forecast of the event is obviously expected, the key point is to explore its accuracy and how this varied with the forecast horizon. In the present case, from the point of view of, e.g., the Galapagos, we have two different forecast ranges. The first one, in a way simpler, concerns the advection phase of the storm we have described in Section 4. Once the swell is generated and on its way, forecasting its arrival is only an oceanographic problem. When extended to five or six days, and on large oceanic distances, the problem is not trivial, and indeed it has received much attention over the years. Without going here into details, we recall the excellent progressive solutions by Booij and Holthuijsen (1987), and Tolman (2002).

A more extended forecast range, on the other hand, also concerns the

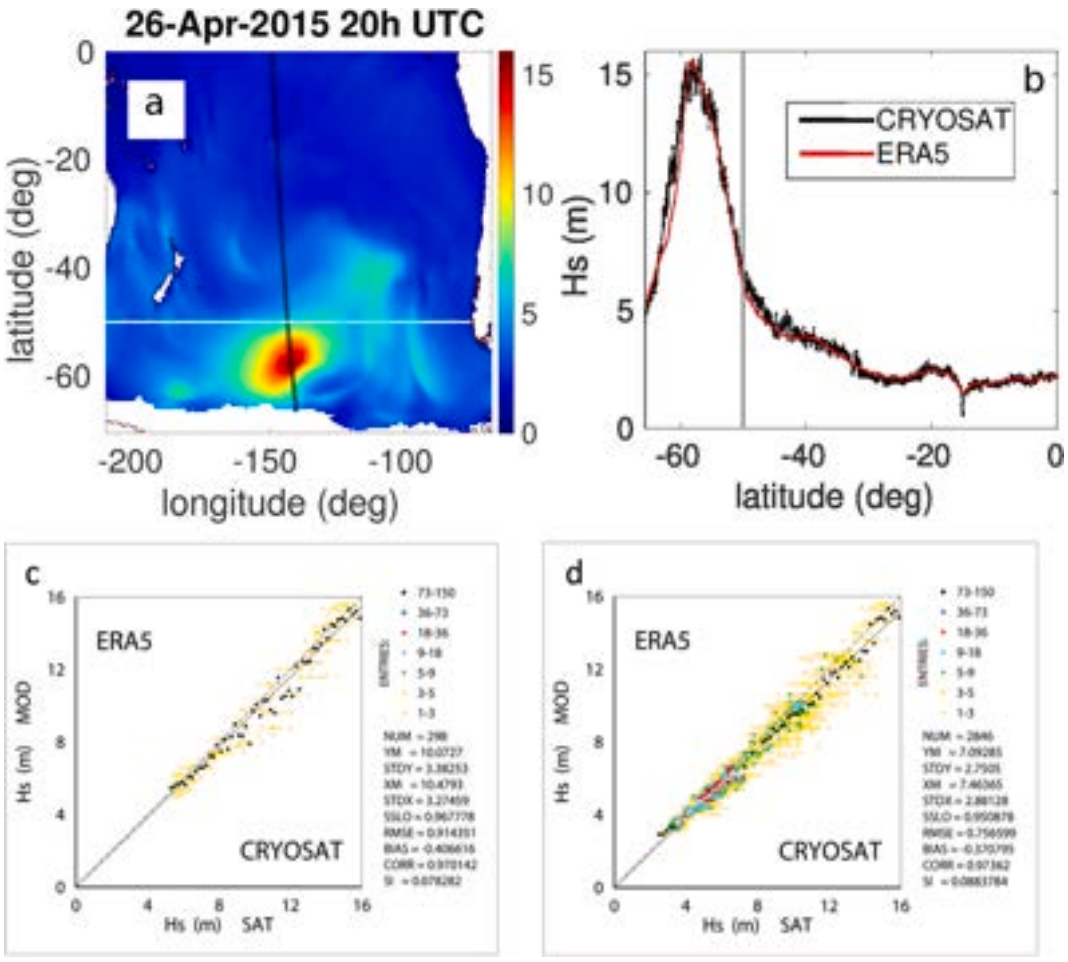

Fig. 5. Comparison between ERA5 derived wave fields and CryoSat-2 altimeter data (south of 50°S). Panels a, b show one pass (black line) whose comparison results are in panel c. Panel d summarizes the statistics out of ten passes during the generation phase of the storm. The statistics are reported in Table 1.

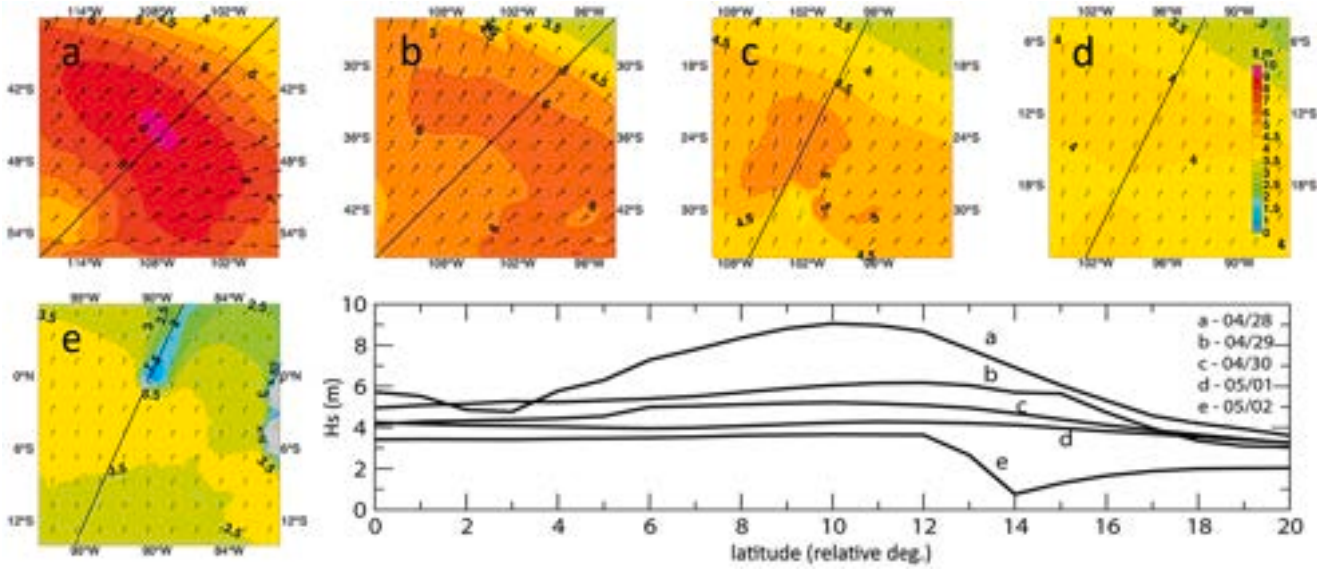

Fig. 6. Advection phase of the event. The progressive areas (see Fig. 1 for their geographical locations) are at 24-hour intervals. Time is 00 UTC, days are in the elongated panel. In each square, the thin line is aligned with the main wave direction. Waves reach the Galapagos in panel e. The long panel provides the significant wave height profile along the various panels, each one spanning 20°in latitude.

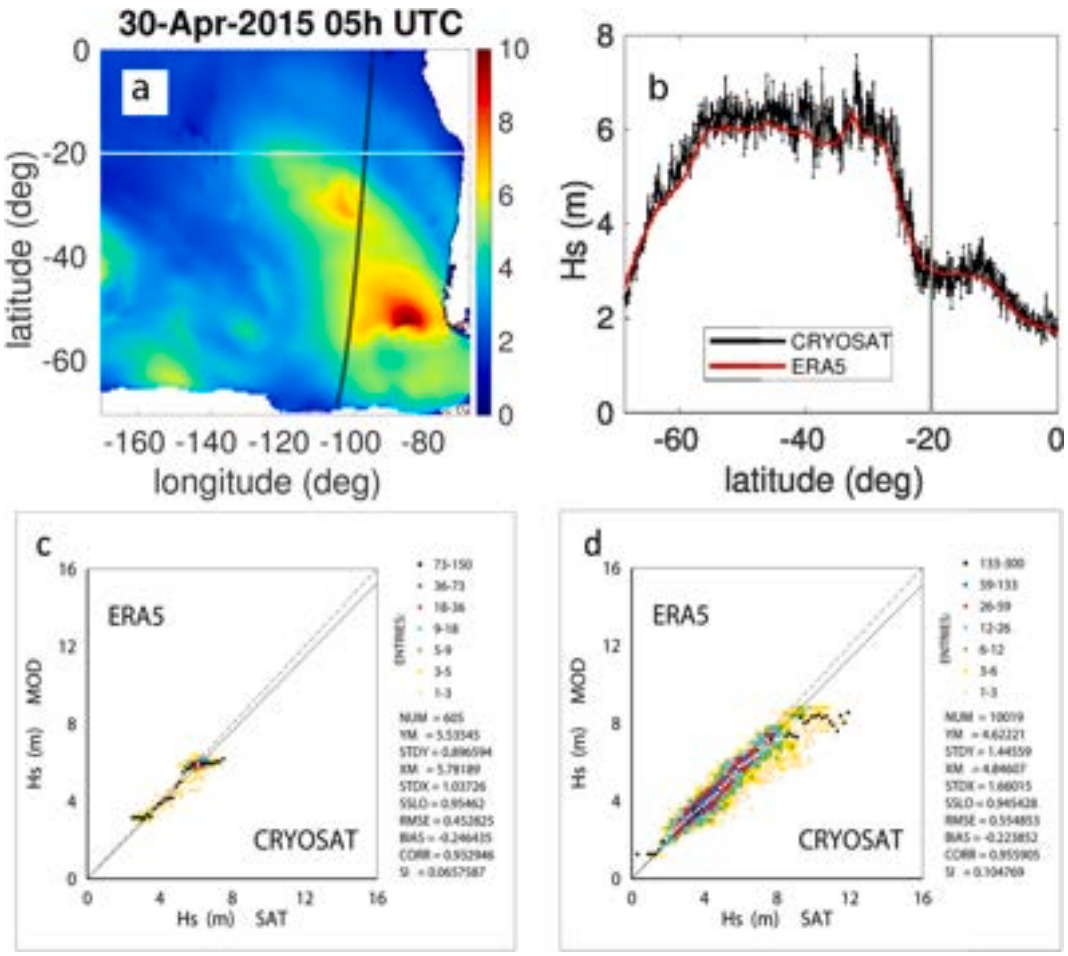

Fig. 7. Comparison between ERA5 derived wave fields and CryoSat-2 altimeter data (south of 20°S). Panels a, b show one pass (black line) whose comparison results are in panel c. Panel d summarizes the statistics out of ten passes during the advection phase of the storm. The statistics are in Table 2.

Table 2
With reference to Fig. 7, statistics of the comparison between model values versus CryoSat-2 altimeter (wave height) data. Dates are 27 April – 02 May 2015. The focus is on the advection area.

sig. wave height	H_s (m)	bias (m)	corr	SI (%)	sslo
1 pass	5.78	−0.25	0.93	6.6	0.95
10 passes	4.85	−0.22	0.96	10.5	0.94

generation phase of the storm (see Section 3). Given the data available, for the Galapagos we limit ourselves to the advection phase, also implying the storm forecast when dealing with the buoy data.

We begin with panels a, b of Fig. 11 showing the time evolution (48 h, 01-02 May) of H_s, T_p at the Galapagos. Note that, not having to deal with satellite data, we use the TL1279 results, hence the higher maximum H_s values compared to the previously mentioned 3.15 m of the ERA5 hourly spectra. We show the analysis and the forecasts up to 4 days (with respect to the control time in the panels). Note that, while the TL1279 analysis (black dots) is archived only for 00-06-12-18 UTC (hence the use of ERA5 where necessary), the forecasts are available at hourly intervals.

It is evident that there is hardly any H_s difference among analysis and forecasts, with only some minor difference in the arrival time of the swell. Similar results hold for the buoy (panels c, d). Apart from reporting also the local measured data, we explore here the forecast up to the 8-day range. We note that including also the generation phase somehow implies a slight anticipation of the event (a few hours), but possibly also a better fit with the measured H_s.

Of course, these extended forecast differences depend on the generation phase of the storm, something we explore in Figs. 12, 13 respectively for wind and waves. In each figure, the four plots provide the TL1279 analysis fields close to the peak conditions and the 1, 2, 3-day forecasts. Note the 6-hour difference between the wind and wave peaks. Granted the strong similarity between the analysis and the forecast fields, a quantification is provided in Table 5. There are obvious differences in the details, hence the values of the scatter index SI, but the general structure of the storm was well predicted up to at least three days in advance. This is more the case for wave heights that, being an integrated quantity, tend to smooth the minor differences present in the wind fields.

A different overall view of these wind and wave fields is provided in Fig. 14. Here we show the growing phase of wind and wave conditions during April 26, according to the analysis and the forecasts issued at 00, 24 and 48 h earlier, on April 25 and April 24, respectively. Still focusing on the area of Figs. 12, 13, the panels show a) the evolution of the maximum and mean wind speeds, b) the maximum and mean significant wave heights, c) the peak and mean wave periods. The black dots represent the analysis data. Granted the actual formal statistics (six parameters, three forecast ranges), we leave the judgment to the reader. Our qualitative assessment is that, with the expected variability, the forecasts were sound, hence the good forecasts seen at the buoy location in panel 11c.

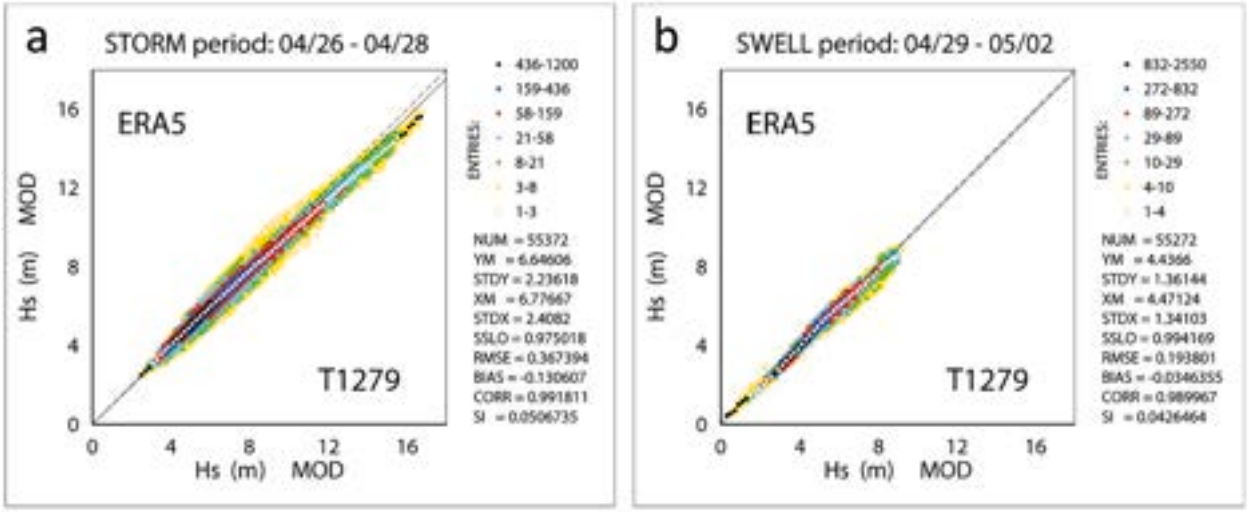

Fig. 8. Comparison between the significant wave heights obtained using ERA5 and T1279 wind fields. Panels a, b are for the stormy and advection phases of the event, respectively. Full statistics are in Table 3.

Table 3
Comparison between the ERA5 significant wave heights versus the TL1279 values (reference). Different statistics are provided for the stormy period (25–26 April) and the advection (swell) period (27 April – 02 May). See Fig. 8 for the graphs.

	H_s (m)	bias (m)	corr	SI (%)	sslo
storm	6.78	−0.13	0.99	5.1	0.97
swell	4.47	−0.03	0.99	4.3	0.99

7. The maximum wave heights

In the previous figures (see in particular Fig. 11), we have seen the evolution of the significant wave heights H_s at the Galapagos. Now we explore which may have been the corresponding maximum single wave heights. Although several formulas exist for this purpose (see, e.g., Benetazzo et al., 2017), we follow a more general approach.

Indeed, the model spectra represent the most likely energy distribution (with frequency) at given time and position, and we have this information at hourly intervals during which we assume for each hour constant conditions (on average). Before the interaction with the islands, conditions vary mildly in space. Hence we focus on a given position (1.48°S, 91°W) as representative for the area. The specific local conditions have been explored reconstructing by linear superposition 1000 different time series for each spectrum whose H_s was $\geq$ 2.5 m, randomizing both the phase of the single spectral components and their amplitude, the latter according to confidence limits (see, among others, Young 1994). From each time series (14400 values at 0.25 s interval) and following also the related contributions by Boccotti (2000), we derived the associated H_{max}, the highest wave in each hour record. We ended up with 48 H_{max} sets, starting at 19 UTC May 01, ending at 18 UTC May 03. The peak conditions of $H_s = 3.15$ m were at 15 UTC on May 02.

For each hour, we derived H_{max}_90, i.e. the wave height exceeded with 90% probability; similarly for H_{max}_50 and H_{max}_10. The results are shown in Fig. 15 for the 48 h between the two indicated time limits.

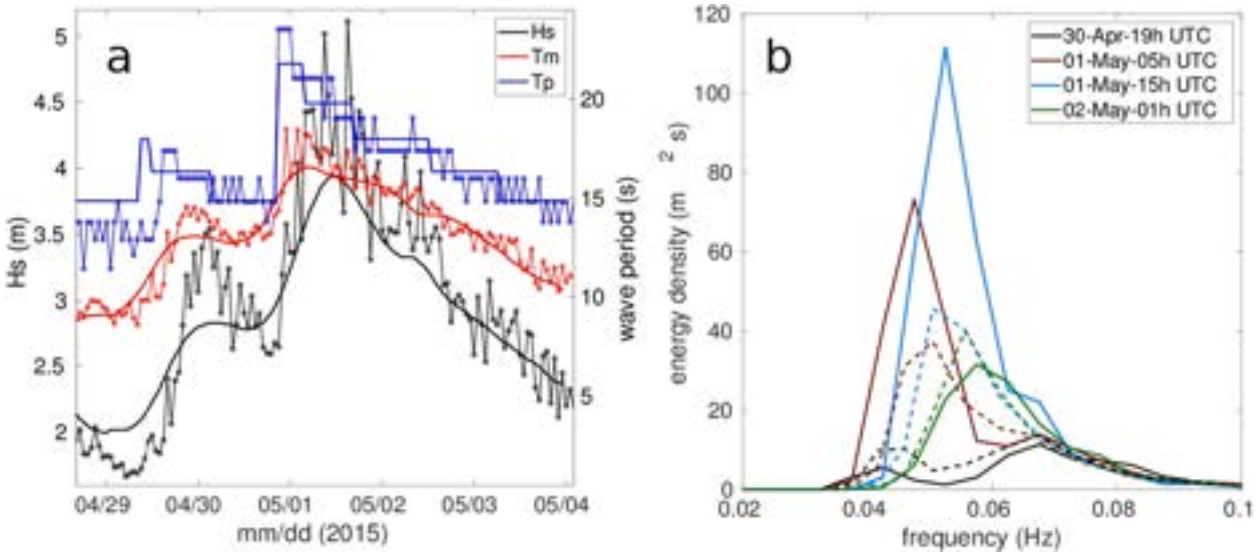

Fig. 9. Comparison between ERA5 derived wave fields (with the extended low-frequency limit – see Section 2) and the highly variable buoy recorded data. See Fig. 1 for its position. Panel a is H_s, T_m, T_p history from 29 April till 04 May. Full statistics in Table 4. Panel b provides a comparison of four respective 1D spectra at ten-hour intervals. Buoy: continuous lines; model: dashed lines.

Table 4
Statistics of the comparison between the ERA5 wave model results and the buoy data. The period is 29 April – May 04. See Fig. 9 for the corresponding graphical data. Buoy position is in Fig. 1.

	buoy	bias	corr	SI (%)	sslo
H_s (m)	2.98	−0.10	0.94	11.6	0.95
T_m (s)	13.3	−0.2	0.95	5.9	0.98
T_p (s)	16.4	0.3	0.87	7.9	1.02

For the combined probability to exceed, at least once, a given H_{max} value throughout the event, we obtain:

$$p_{Hmax} = 1 - \prod_{i=1}^{48}(1 - p_i)$$

where p_i is the occurrence probability for each single hour.

The overall results are shown in Fig. 16. We see at once that a prolonged 3.15 m maximum H_s swell, taking the overall evolution into account, can lead to quite large single wave heights. We stress that the particularly high values are associated to swell conditions. This implies a high correlation (Boccotti, 2000) between a high crest and the depth of the associated troughs, hence more likely large wave heights.

8. The distribution of swell

Numerical models provide a quite realistic distribution of swell over time. Indeed, a sequence of maps as in Fig. 17 provide at the same time a beautiful and effective way to show how the large swell system propagates and attenuates in time. Other, less relevant processes, as viscous

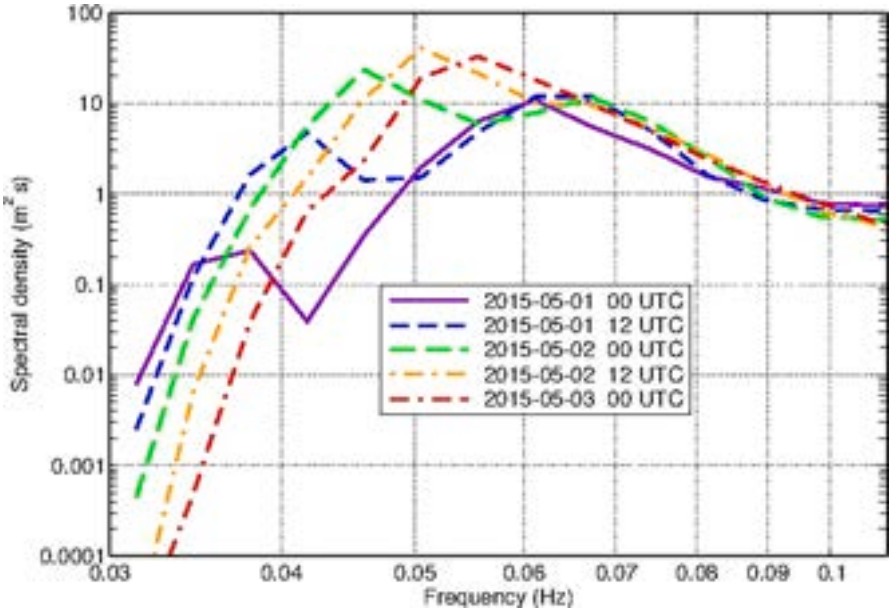

Fig. 10. Evolution, 1 D spectra at 12-hour intervals, of the ERA5 wave conditions at Galapagos. Logarithmic scales are used to better highlight the incoming forerunners in the early phase of the local high sea conditions. Note the extremely low frequencies, visible (see Section 2) because of the extended low-frequency range.

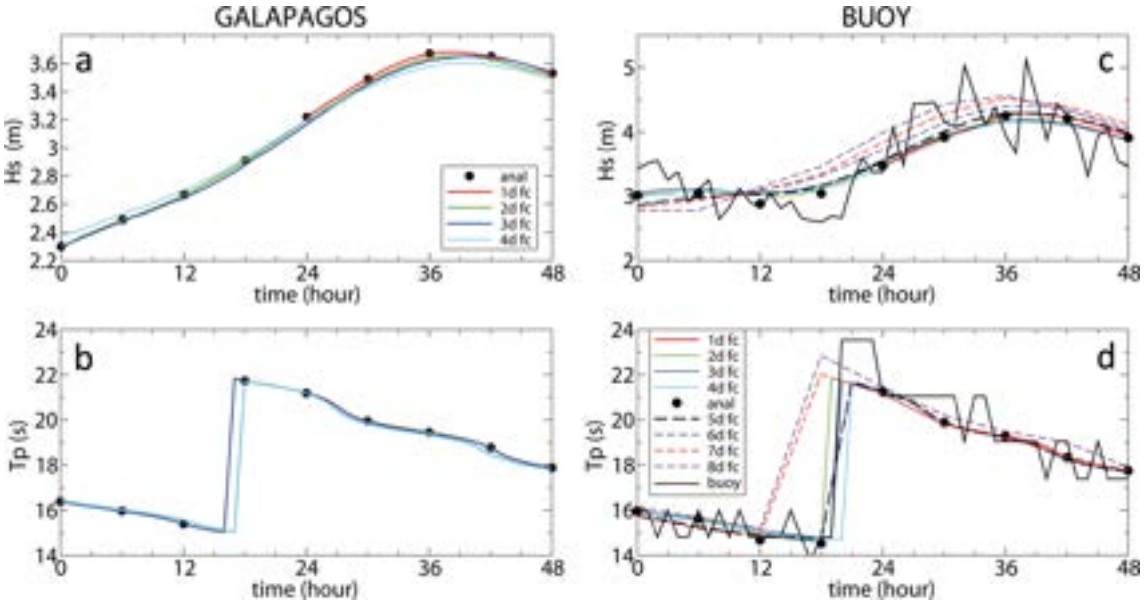

Fig. 11. Comparison, for H_s and T_p, between the analysis data and 1, 2, 3, 4 day forecasts at Galapagos and the buoy. See Fig. 1 for their geographical locations. For the buoy, for which also measured data are shown, the forecast is extended to 8 days before the local event.

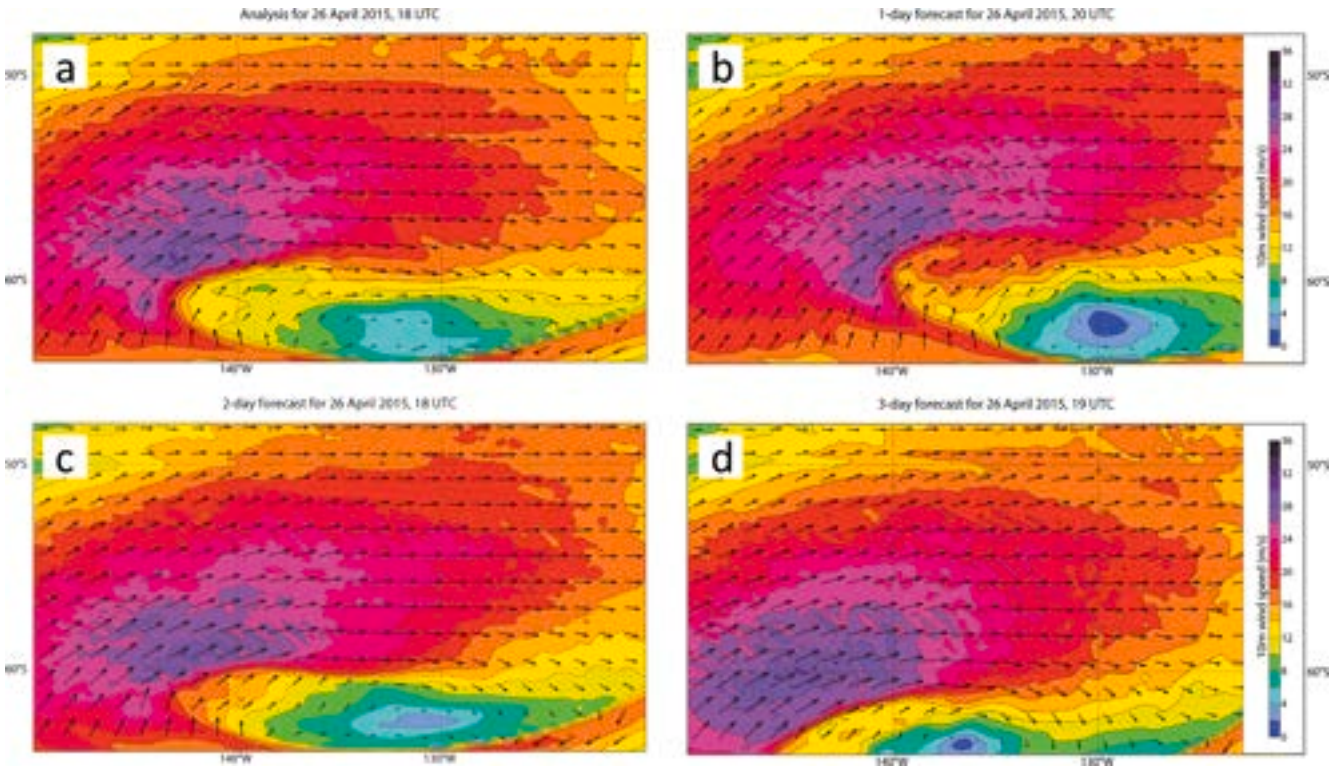

Fig. 12. Peak wind conditions. Time is 25 April, 18 UTC. Panel a, analysis. Panels b, c, d 1, 2, 3 day forecasts, respectively. See Fig. 1 for the geographical location. The related statistics is in Table 5.

dissipation (Babanin, 2011) or momentum pumping to the atmosphere (Ardhuin et al., 2009), are at work. However, by far the main reason for a decrease of the swell height in time is its dispersion on an ever-increasing area. On this basis and neglecting the less relevant processes (together with the possible interaction with another storm), we have looked for a quick and practical "rule of thumb" approach to

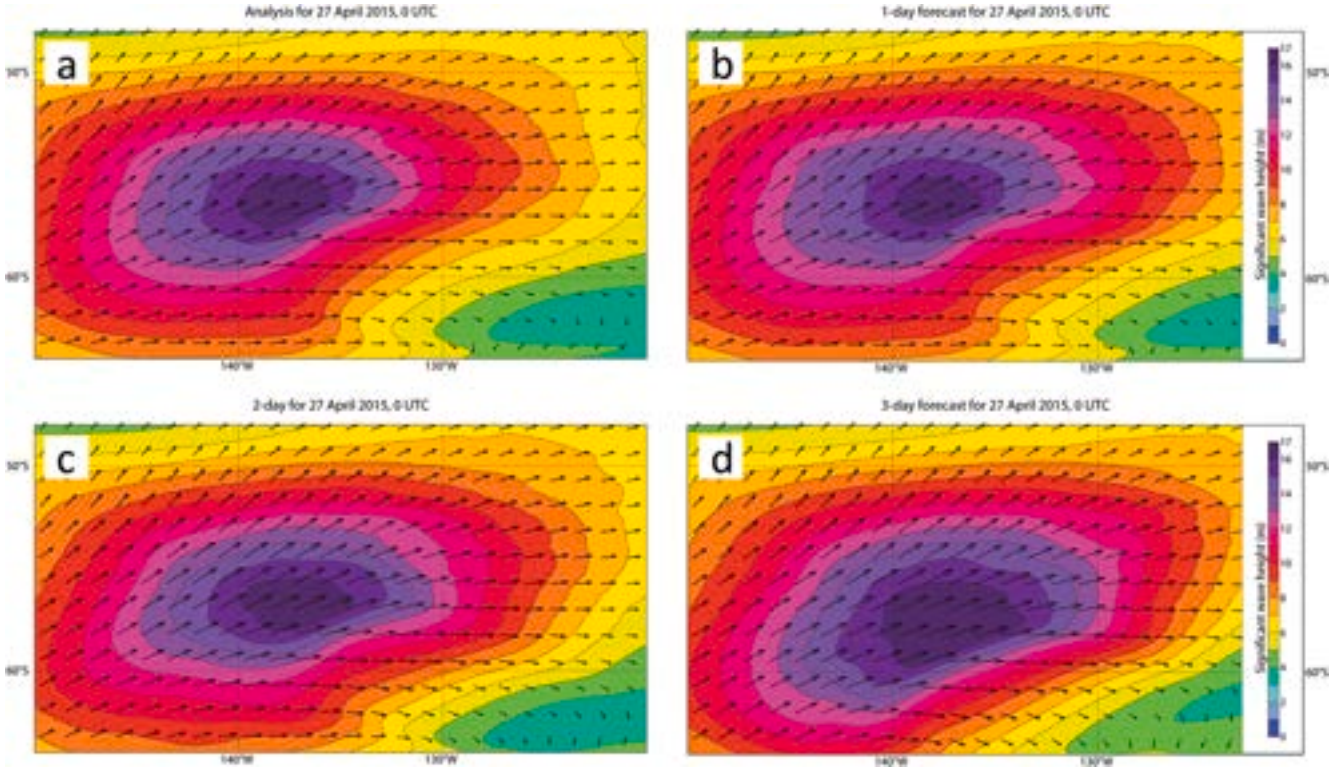

Fig. 13. Peak wave conditions. Time is 26 April, 00 UTC. Panel a, analysis. Panels b, c, d 1, 2, 3 day forecasts, respectively. See Fig. 1 for the geographical location. The related statistics is in Table 5.

Table 5
With references to Fig. 12 (wind speed) and Fig. 13 (significant wave height), statistics of the (overall maps) comparison of the various forecasts (1, 2, 3-day range) versus the corresponding analysis (reference). Time is 25 April 18 UTC for wind, 26 April 00 UTC for waves, corresponding to the respective peak conditions.

	$\bar{U}_{10}$ (ms^{-1})	bias (ms^{-1})	corr	SI (%)	sslo
1 D	13.17	0.11	0.98	8.0	1.01
2 D		0.35	0.94	12.9	1.03
3 D		0.17	0.84	22.0	1.02
	$\bar{H}_s$ (m)	bias (m)	corr	SI (%)	sslo
1 D	6.24	0.07	1.00	3.3	1.01
2 D		0.13	0.98	8.1	1.02
3 D		0.18	0.97	12.5	1.04

estimate how the swell area expands in time and the associated decrease of swell height. In very general terms, we assume a generation area A_0, and, on the basis of some simple, but reasonable assumptions (the details are in the Appendix A), we derive the area A_1 covered by the propagating swell at time t. Given the maximum H_{s0} in and at A_0, we derive the maximum H_{s1} as:

$$H_{s1} = H_{s0} \cdot \sqrt{A_1/A_0}$$

Applied to the Galapagos case, the results, up until the impact on the islands, are in Table 6.

We do not claim that such accuracy can be a general result as it depends on the specific conditions and the present case is an almost ideal situation. However, from a couple of extra tests we did we believe that a 10–15% approximation is a reasonable assumption for a quick estimate.

9. Discussion and Conclusions

It is now time to summarize and discuss our findings, complementing this with some further considerations.

To begin with, we stress the peculiarity of the storm once again. Indeed, as discussed, it is possible this was also due to a more northerly track of the storm with respect to the average flow in the Antarctic belt, bringing the storm in an area of warmer ocean water. Of course, this led to an enhanced heat and energy flow to the atmospheric system, with also enhanced air-sea instability conditions. From the atmospheric point of view, this favoured the presence of gustiness in the wind field, which may have positively contributed to the wave growth. From the ocean point of view, the data suggest that the peak of the storm moved with a

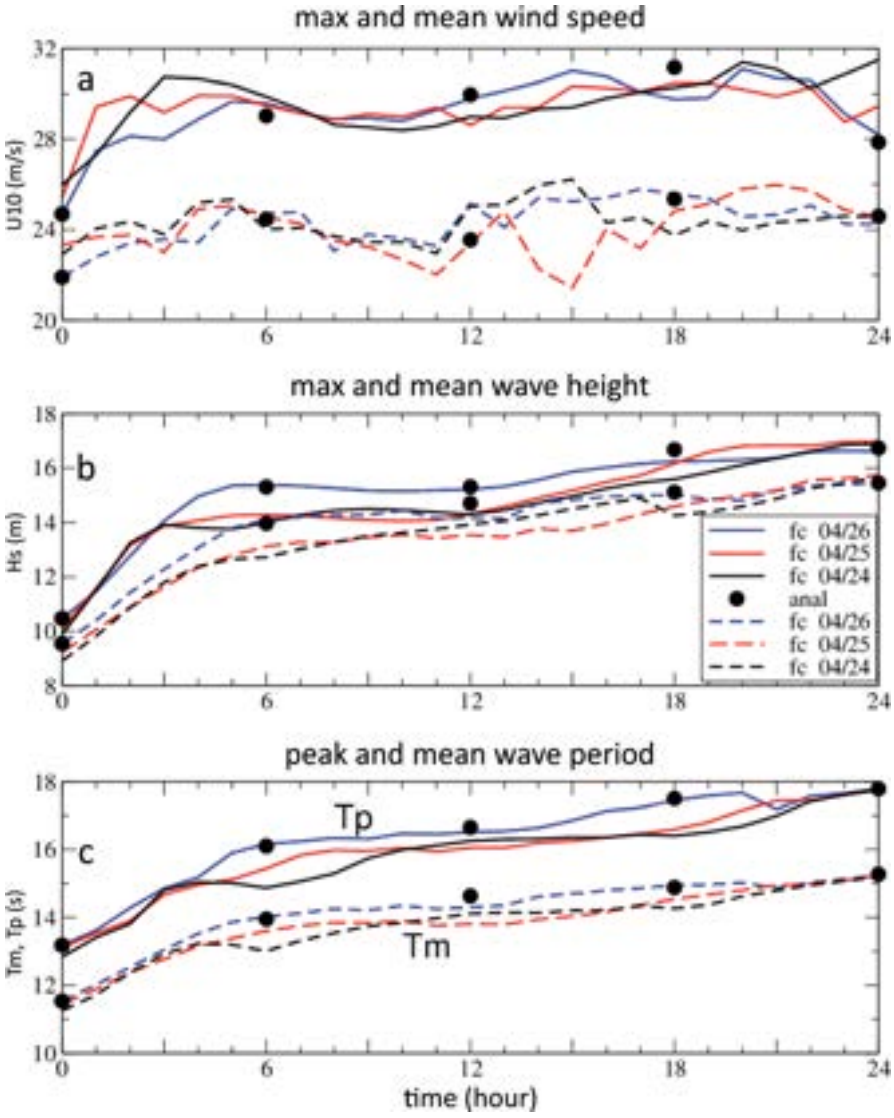

Fig. 14. Wind and wave conditions during the growth phase of the storm. The plots show the peak and mean, wind and wave, conditions out of Figs. 12 and 13. Dots are analysis data. 1, 2, 3 day forecasts are shown.

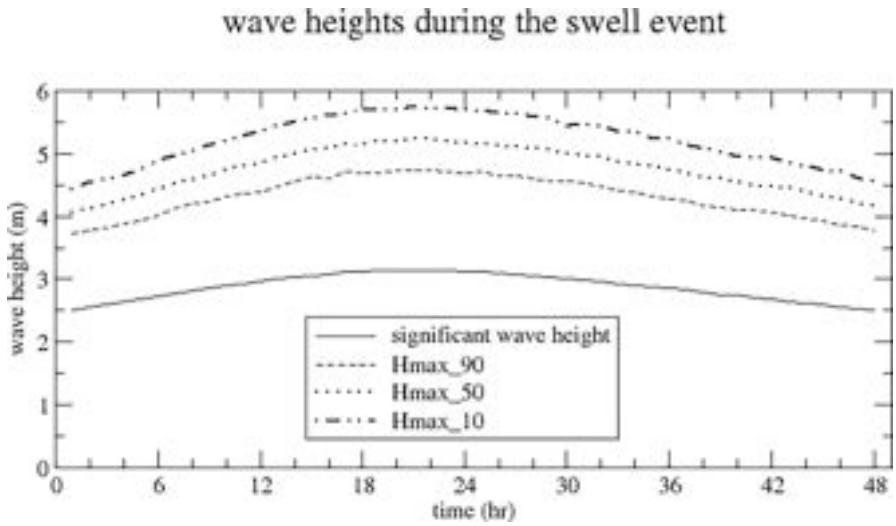

Fig. 15. Evolution of the wave conditions in front of the Galapagos Islands. The 48 h go from 19 UTC on May 01, 2015 to 18 UTC on May 03, 2015. Hmax_XX show the single maximum wave height with XX% probability to be exceeded during the single hours.

speed close to the group speed of the dominant waves, which led to dynamical generation and the extended very high peak conditions of the storm.

In Section 4, while discussing the advection phase, and comparing in Fig. 7 altimeter and model swell data (see panel a), we pointed out the presence of a higher wave heights zone at about 20° S, 100° E. The analysis of the meteorological maps reveals the presence of an unusual tropical storm, Katie, at this location. More information can be found in Young (2016). Although peculiar, Katie was not very intense, its maximum wind speed being close to 15 ms^{-1}. This could hardly have any relevant effect on a 20 sec, or more, swell moving at 30 ms^{-1} or faster. However, it produced some local wind sea, hence the locally higher significant wave heights. The consequences were the anomalous altimeter peak in panel b and the off-the-best-fit-line isolated data in panels c, d. All this clearly implies that the model, in this case ERA5, did not pick up properly the Katie structure. This is not surprising given the ERA5 31 km resolution. All this is not relevant for our present purposes.

A macroscopic feature we pointed out, especially in Fig. 9, is the strong variability of the recorded data around their general trend. While this can somehow be expected for the peak period because of its defined discrete values, it may appear surprising in the H_s record. A short clarification is due. Every 20- or 30-minute record, with about 100 or 200 waves depending on the conditions, provides only an estimate of the significant wave height and, even more so, of the related spectrum. In average conditions, we must expect at least a 6% rms variability for H_s records taken in similar conditions. Donelan and Pierson (1983) provide a full discussion of the subject. However, in our case conditions are much worse. First of all, our waves are very long, with a 20 s dominant period or more. This implies that in 20 min we measure only 60 waves or so, significantly increasing the variability of the integral parameters. Additionally, with the narrow spectrum that characterizes the high long swell, groups were very long, possibly with ten or fifteen waves or more, which implied long time intervals between a sequence of low waves and the following peak of the group. With possibly four or five groups in a record, the resulting H_s much depends on when we randomly initiate and end a record. The practical consequence is the variability we find in the buoy records. Note that this is also reflected in space, hence the enhanced variability of the altimeter data.

A relevant question is to estimate how high the maximum waves were on the Galapagos coasts. Ignoring here the local features and focusing on the 48 h when the significant wave height was $\geq$ 2.5 m, we have performed a specific analysis in this respect. First, we have randomized the possible one-hour time series and derived the associated statistics. The results, in Fig. 15, show that the coasts of the Galapagos

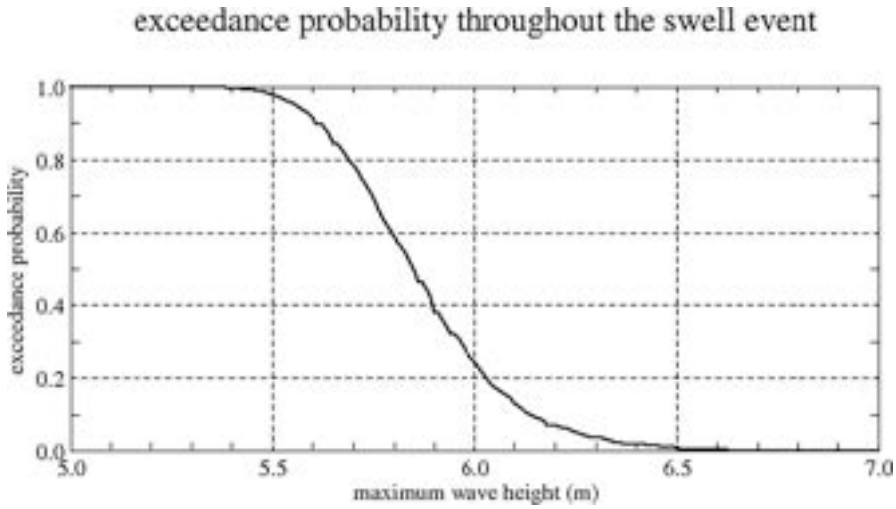

Fig. 16. With reference to the 48 h in Fig. 15, overall exceedance probability (e.g., 0.4 = 40%) for a given single wave height throughout the considered period.

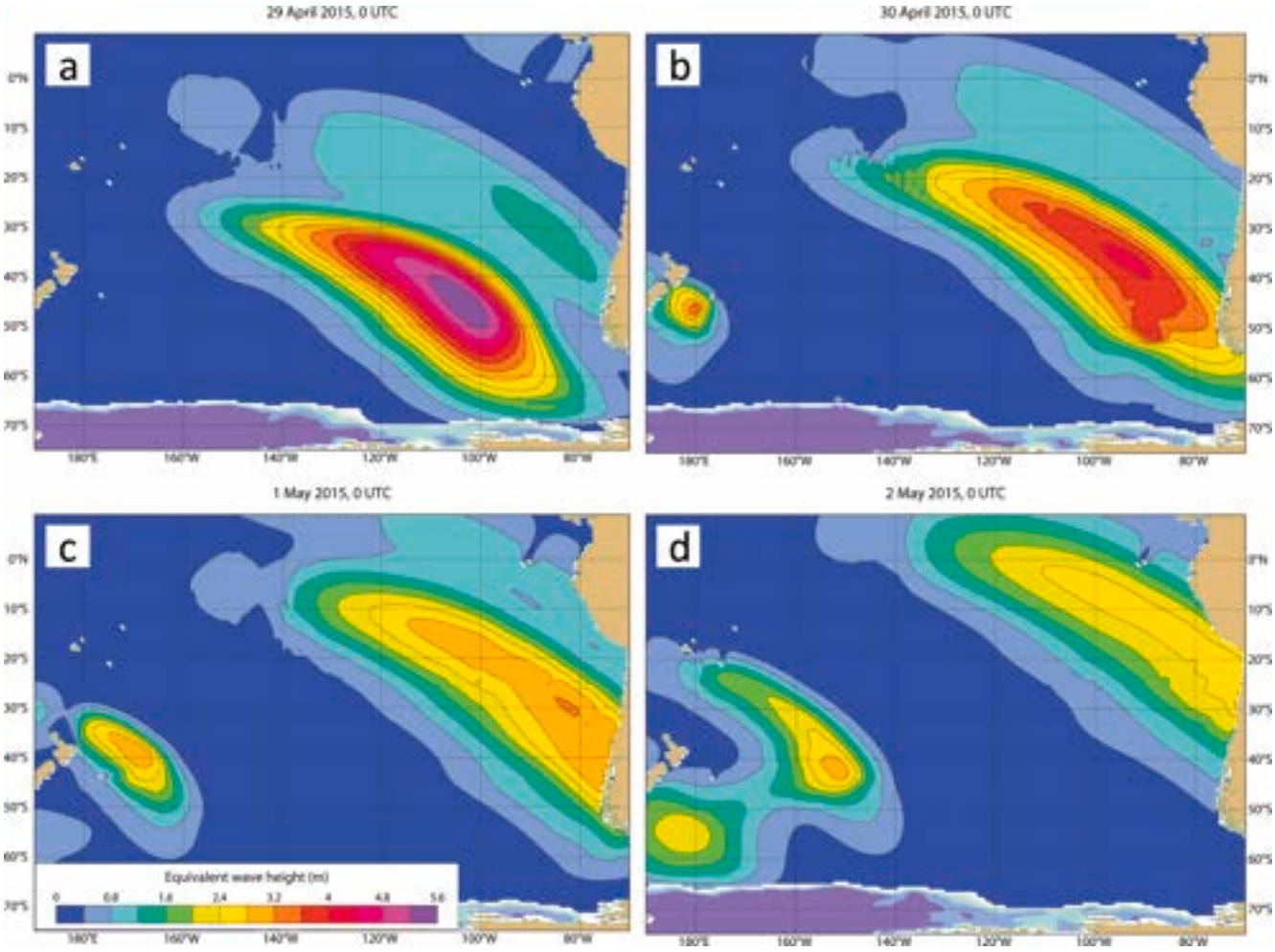

Fig. 17. Swell propagation in the Southern Pacific Ocean as depicted by the equivalent significant wave height of all waves with periods between 17 and 21 s. Panels a - d are at 24-hour intervals. Note the beginning of the interaction with the Galapagos Islands (panel d, upper right).

had to withstand large single wave heights, with 10% probability close to 6 m, in contrast to the typical local value of 1.5 m. This holds singularly for each hour. The expected H_{max} are larger (see Fig. 16) if we consider the combined probability throughout the swell event.

Granted the relevance and accuracy of the model results, we also suggest a simple, but sound approach to estimate the evolution in time of the peak H_s of the swell with a straightforward calculation. This is based on overall energy conservation distributed on a progressively expanding area. We describe the procedure in the Appendix A. The results for the Galapagos swell under discussion (see Table 6) are surprisingly good.

An interesting, although perhaps academic, point is the local information provided by the initial very low-frequency waves, with peak periods between 20 and 30 s (see Fig. 10). Such waves do not arise out of the blue, and were themselves a strong indication that somewhere there

Table 6
Evolution, in time, of the distance run, and the area covered, by the swell, of its estimated maximum significant wave height versus the corresponding model estimate.

Southern Pacific Ocean
Swell distribution over 5 days, starting time 00 UTC April 27, 2015
Initial area 15.0 × 12.0 deg (lon, lat)
Initial Hs 16.0 m
Initial T_p 18.0 s

day	distance (1000 km)	area (1000 km)^2	H_s_max (m)	model H_s_max (m)
0	0	2.22	16.00	16.00
1	1.213	6.74	9.18	9.06
2	2.426	13.44	6.50	6.06
3	3.639	22.32	5.04	5.22
4	4.852	33.37	4.12	4.28
5	6.065	46.61	3.49	3.60

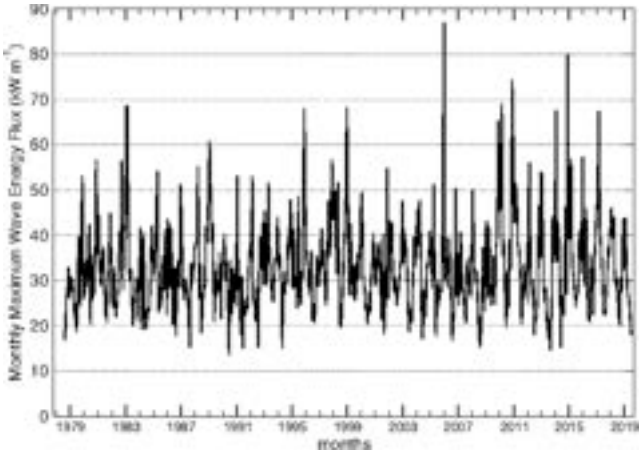

Fig. 18. Monthly maximum of wave energy flux at Galapagos from 1979 till 2019. ERA5 driven wave fields (ecWAM CY47R1), (see Section 2), but with an extended low-frequency limit. Note the two peaks in 2006 and 2015, the latter the one here analysed.

had been a very strong storm, and that something heavy was on its way. Apart from the required oceanographic knowledge, it would not be easy to detect these long waves without instruments and the related analysis. However, the information was potentially there and, apart from model forecasts, this is something to keep in mind. In this respect it is interesting to quote the experience of the Polynesian navigators who, lying on their boat and feeling its motion, were able to recognize the characteristics (height, period and direction) of various superimposed swell systems. The interested reader can find a good reference in Lewis (1994).

A relevant question is whether the 2015 event was unique or, more simply, a relevant, but rare, episode. Pursuing this idea, we have explored the Galapagos wave climatology using the ERA5 data from 1979 through 2019 (forty-one years). The time series of the monthly maximum wave energy flux (kWm^{-1}) is provided in Fig. 18. There is obviously the 2015 peak, but we see a higher peak nine years earlier. We did not explore this previous event, but it is instructive to note that the 2015 one was not, as often claimed, something that had "never been seen before".

From the point of view of the local islanders and activities, an effort should be performed for the information to reach the local users and interested authorities. The information exists, from different sources, and it is available, so it seems absurd in present times not to take advantage of them. Of course, there is also the problem of the return-time of these unusual events and of the constructions where "constructions should not be". This is a more general problem that we do not touch here. Rather, it is time to summarize the main points and findings in this paper. This is done in the next, final section.

10. Summary

We itemize here the main findings of this paper.

(1) A particularly intense Antarctic storm has been analysed. The storm sent large swell throughout the Southern Pacific Ocean.
(2) A possible reason for the very active meteorological conditions was the more northern path of the storm and the interaction with an unusually warm ocean area.
(3) This not only led to a stronger meteorological event, but it also created the conditions for more active wave generation. The latter was further enhanced because the wave peak area was moving along with a speed similar to that of the meteorological storm (dynamical generation).
(4) Modelling of both meteorological and wave events was done using both ERA5 and the then operational TL1279 prediction system, and the corresponding ecWAM wave model. A devoted ecWAM run was done extending the frequency range further towards the lower frequencies.
(5) Validation has been done using scatterometer, altimeter and (one) buoy data. ERA5 results appear slightly underestimated (a few percent), particularly in the high value range. The TL1279 results are much closer to the measured data.
(6) The swell took almost five days to reach the Galapagos, decreasing its height while spreading over progressively wider areas.
(7) At the Galapagos, the maximum significant wave height was estimated at more than 4 m, with 20 s period. The first forerunners were up to about 27 s.
(8) Comparison with measured data at the WHOI-32012 buoy suggests that the overall event was modelled correctly, but with a likely underestimation of the peak significant wave height.
(9) Granted the modelled H_s history at the Galapagos, we have also estimated the evolution of the likely maximum wave height at every stage of the event. We have also estimated the exceedance probability of various extreme H_{max} levels. Should the possible underestimation cited at point 8 be true, these values should be correspondingly increased.
(10) The long dominant wave periods and the peakedness of the spectrum led to very long beat periods. This implies an enhanced variability of the buoy measured wave heights and periods.
(11) Starting from a given generation area, an expression has been derived to provide a crude estimate of the progressively expanding swell area and of the associate peak conditions.
(12) Very low frequency (0.035 Hz) forerunners reached the Galapagos the day before the peak conditions. The information was significant for what was about to come, but its perception was a very difficult task, and it was not used.
(13) However, more formal forecasts were available, both after the swell was on its way (five days before reaching the Galapagos) and also involving the generation phase (eight days before).
(14) This information was not used. An effort should be done to convey the information to the local users and authorities.
(15) Although rare, the swell event was not unique. Analysis of the local ERA5 history indicates that an apparently stronger event happened in 2006.

CRediT authorship contribution statement

L. Cavaleri: Conceptualization, Methodology, Formal analysis, Writing – original draft, Supervision. **A. Benetazzo:** Validation, Writing – review & editing. **L. Bertotti:** Software, Writing – review & editing, Visualization. **J.-R. Bidlot:** Methodology, Formal analysis, Writing – review & editing, Visualization. **A. Pomaro:** Writing – review & editing, Visualization. **J. Portilla-Yandun:** Software, Formal analysis, Writing – review & editing, Visualization, Funding acquisition.

Declaration of Competing Interest

The authors declare that they have no known competing financial interests or personal relationships that could have appeared to influence the work reported in this paper.

Acknowledgements

J. Portilla-Yandun acknowledges EPN project PIGR-19-08. This work has also been conducted as part of the bilateral project EOLO-1 ("Extreme Oceanic waves during tropical, tropical-like, and bomb cyclones") between CNR-ISMAR and the University of Tokyo (Japan). The buoy data have been retrieved from the NOAA-NDBC archive https://www.ndbc.noaa.gov. Satellite data was downloaded from the IOWAGA archive at https://wwz.ifremer.fr/iowaga/Products. Following the rules of the European Centre for Medium-Range Weather Forecasts, the model data are available at the Centre. More specifically:

– the wave hindcast with 37 frequencies at https://doi.org/10.21957/9jcv-r297 ,

The long wave hindcast was created using four experiments. The results for the single decades are available at:

– 1979-1989 at https://doi.org/10.21957/y03s-tz09.
– 1990-1999 at https://doi.org/10.21957/strn-cs36.
– 2000-2009 at https://doi.org/10.21957/dgkx-1485.
– 2010-2020 at https://doi.org/10.21957/t3vj-b111 .

Silvio Davison has done a careful review of the English text that we much appreciate.

Appendix A

The propagation and attenuation of swell in time.

A.1. Our purpose

We aim at formulating a simple "rule of thumb" approach to estimate with a pocket calculator formula the basic characteristics of a swell area, namely its expansion and the maximum significant wave height, respectively growing and decreasing in time. We start from the stormy area, with given angular amplitude and peak conditions, and aim at quantifying how they evolve in time. At this purpose we start in A2 with a single point generation. In A3 and A4 we consider respectively large, rectangular and elliptical, generation areas. In A5 we sketch some practical considerations.

A.2. Single point generation

We assume a JONSWAP spectrum (Hasselmann et al., 1973) at a stormy single point area (point A in Fig. A1). We assume a $\cos^4$ directional energy distribution. For a given peak period T_p we consider the section of spectrum in the $0.5\ T_p - 1.4\ T_p$ (i.e. $0.7\ f_p - 2\ f_p$, with $f_p = 1/T_p$ the peak frequency). A straightforward calculation shows that this range includes 96% of the overall energy. Further, for practical purposes we consider the $\pm 30^\circ$ directional range (0° the main flow direction). On the whole these two limitations include 75% of the overall energy.

In Fig. A1 $x = \overline{AB} = \overline{AD} = \overline{AC}$ represents the general distance run by the peak frequency components after a certain time. We assume that at this stage the energy is distributed on a curved ellipsoid area, whose (curved) axis is $\widehat{BDC}$. The "external" area (//////////) is where the faster wave components have arrived. The "internal" one (\\\\\\\\\\) shows the area of the slower (than the peak) ones. Ignoring the curvature (in the first order the external and internal parts errors compensate each other), the area covered by the swell is:

$$A_{sw} = \widehat{BDC} \cdot 0.4 \cdot x \cdot \pi/4 + \widehat{BDC} \cdot 0.5 \cdot x \cdot \pi/4$$

Noting that $\widehat{BDC} = (\pi/3) \cdot x$

$$A_{sw} = 0.74 \cdot x^2$$

With g the gravity acceleration 9.81 ms^{-2},

$$x = (g/4\pi) \cdot T_p \cdot time (\text{units m, s})$$

$$= 0.78 \cdot T_p \cdot time$$

Hence.

$$A_{sw} = 0.45 \cdot T_p^2 \cdot time^2 (\text{units m, s})$$

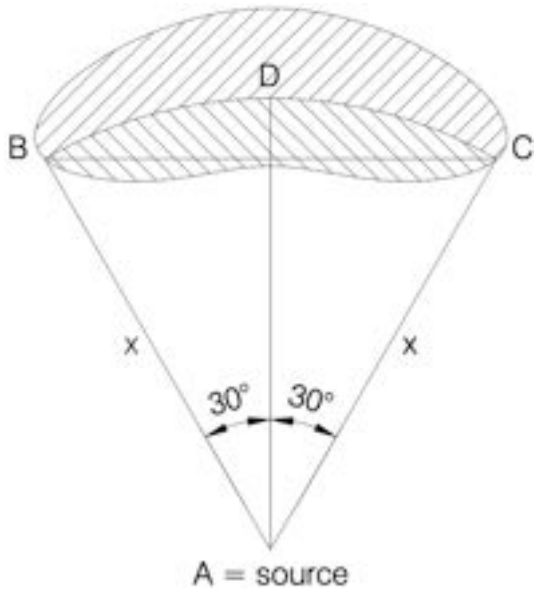

Fig. A1. Swell propagation from the single point A. See text (A2) for the details.

A.3. Rectangular area generation

We now consider a stormy area with dimensions (see Fig. A2) d, c (respectively longitude and latitude). Following the logic in A2, the swell area after a certain time (distance x) is given by the curved "rectangle" AEFDHONL plus the "external" and "internal" curved half-ellipsoid areas. Simple geometry suggests $c\cdot(d+x)$ as area of the bent rectangle. Besides we have the ellipsoid area of Section A2 plus the d-wide ones external (from E to F) and internal (from N to O) to the curved rectangle. On the whole this leads to:

$$A_{sw} = 0.74\cdot x^2 + 0.9\cdot d\cdot x + c\cdot(d+x)$$

$$= 0.74\cdot x^2 + (0.9\cdot d + c)\cdot x + c\cdot d \quad \text{(a1)}$$

with $x = 0.78\cdot T_p\cdot time$ (units m, s).

Under the (first order approximation) assumption that energy spreads uniformly in space and time, after a *time* (s) with T_p (s) initial peak period, the maximum swell height is given by:

$$H_{sw} = H_{smax}\cdot(c\cdot d/A_{sw})^{0.5}$$

with H_{smax} the peak significant wave height in the storm.

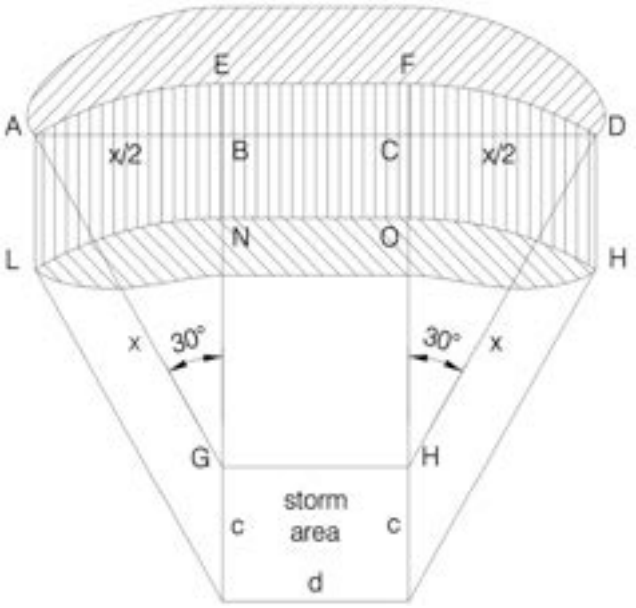

Fig. A2. Swell propagation from the initial storm area. See text (A3) for the details.

A.4. Elliptical area generation

With similar geometrical considerations, starting with an elliptical stormy area (axes c, d as in Fig. A2), we reach the similar expression.

$$A_{sw} = 0.70\cdot x^2 + (\pi/4)\cdot(0.9\cdot d + c)\cdot x + (\pi/4)\cdot c\cdot d \quad \text{(a2)}$$

A.5. Some general suggestions

As seen in Table 6 in the main text, applying the above formulas (we used the rectangular one, but there is not much difference – see below) we obtained surprisingly good results. As there said, this was a practically ideal case, that on the other hand is what we have here considered. There is a key point that we explain. The area expands in time, this is obvious. The question is how much in relation to the initial stormy one. Both from Fig. A2, and also from expressions (a1), (a2), it is obvious that the relative expansion will depend on the dimensions of the initial stormy area. In other words, the larger the stormy area, the smaller the relative increase of the swell area, hence the decrease of the internal, in particular the peak, wave height(s). On the other hand, this makes sense, as our intuition suggests. However, this means that we must have an idea about how to select the initial stormy area. Our practical tests suggested that the area enclosed by the $H_{s\_peak}/2$ isoline is a good bet, with H_{s_peak} the maximum significant wave height at the peak of the storm. As seen in Table 6, this was a very large area. On the other hand, this was, if not unique, certainly a very peculiar intense storm, both as geographical extension and intensity, hence the large swell. It is clear that storms with different, possibly more complicated, geometry (the mind goes naturally to hurricanes and typhoons) may behave differently. However, it is possible that a similar analysis provides a similar "rule of thumb" for guessing the swell wave heights further on.

Practicality? Debatable given the widespread use of computer wave models. On the other hand, it is always useful (and we also find personal satisfaction in) being able to guess, practically at once, what the conditions will be without the need of sophisticated models and machines.

References

Abdalla, S., Cavaleri, L., 2002. Effect of wind variability and variable air density on wave modeling, 17–1/17-17 J. Geoph. Res. 107 (C7). https://doi.org/10.1029/2000JC000639.

Ardhuin, F., Chapron, B., Collard, F., 2009. Observation of swell dissipation across oceans. Geoph. Res. Let. 36 (6), L06607 https://doi.org/10.1029/2008GL037030.

Babanin, A., 2011. Breaking and dissipation of ocean surface waves. Cambridge University Press, p. 403.

Benetazzo, A., Barbariol, F., Bergamasco, F., Carniel, S., Sclavo, M., Yoo, J., Cavaleri, L., Kim, S.S., Bertotti, L., Barbariol, F., Shim, J.S., 2017. Space-time extreme wind waves: analysis and prediction of shape and height. Ocean Model. 113, 201–216. https://doi.org/10.1016/j.ocemod.2017.03.010.

Blunden, J., Arndt, D.S., (Eds.), 2016. State of the Climate in 2015. Spec. Suppl. Bull. Am. Met. Soc., 97, 8, 300pp.

Boccotti, P., 2000. Wave Mechanics for Ocean Engineering. Elsevier Science B.V., 496 pp.

Bogen, K.T., Fisher, L.E., Jones, E.D., 2011. Recent hurricane research – climate, dynamics and societal impacts. Ch.5, 103-118, doi: 10.5772/14184.

Booij, N., Holthuijsen, L.H., 1987. Propagation of ocean waves in discrete spectral wave models. J. Comp Phys. 68 (2), 307–326, 10.106/0021-999/.

Donelan, M., Pierson, W.J., 1983. The sampling variability of estimates of spectra of wind generated gravity waves. J. Geoph. Res. 88 (C7), 4381–4392. https://doi.org/10.1029/JC088iC07p04381.

ECMWF, 2020. Official IFS Documentation CY47R1. In chap. PART VII: ECMWF wave model. Reading, UK: ECMWF. https://www.ecmwf.int/node/19751.

Harpp, K.S., White, W.M., 2001. Tracing a mantle plume: Isotopic and trace element variations of Galápagos seamounts. Geochem. Geophys. Geosyst. 2 (6) https://doi.org/10.1029/2000GC000137.

Hasselmann, K., Barnett, T.P., Bows, E., Carlson, H., Cartright, D.E., Enke, K., Ewing, J. A., Gienapp, H., Hasselmann, D.E., Kruseman, P., Meeburg, A., Muller, P., Olbers, D. J., Richter, K., Sell, W., Walden, H., 1973. Measurements of wind-wave growth and swell decay during the Joint North Sea Wave Project (JONSWAP). Deut. Hydrogr. Inst. Hamburg, Roihe A(8o), Nr.12 94.

Hersbach, H., Bell, B., Berrisford, P., Hirahara, S., Horányi, A., Muñoz-Sabater, J., Nicolas, J., Peubey, C., Radu, R., Schepers, D., Simmons, A., Soci, C., Abdalla, S., Abellan, X., Balsamo, G., Bechtold, P., Biavati, G., Bidlot, J., Bonavita, M., Chiara, G., Dahlgren, P., Dee, D., Diamantakis, M., Dragani, R., Flemming, J., Forbes, R., Fuentes, M., Geer, A., Haimberger, L., Healy, S., Hogan, R.J., Hólm, E., Janisková, M., Keeley, S., Laloyaux, P., Lopez, P., Lupu, C., Radnoti, G., Rosnay, P., Rozum, I., Vamborg, F., Villaume, S., Thépaut, J.-N., 2020. The ERA5 global reanalysis. Quart J. Roy. Met. Soc. 146 (730), 1999–2049. https://doi.org/10.1002/qj.3803.

Lewis, D., 1994. We, the navigators: the ancient art of land finding in the Pacific. Univ. of Hawaii, Honolulu, p. 387.

Pierson, W.J., Moskowitz, L., 1964. A proposed spectral form for fully developed wind sea based on the similarity theory of S.A.Kitaigorodskii. J. Geoph. Res. 69, 24, 5181–5190.

Portilla-Yandún, J., Salazar, A., Sosa, J., Latandret, S., Cavaleri, L., 2020. Modeling multiple wave systems in the eastern equatorial Pacific. Oc.Dyn. 70 (7), 977–990.

Rintoul, S.R., Chown, S.L., DeConto, R.M., England, M.H., Fricker, H.A., Masson-Delmotte, V., Naish, T.R., Siegert, M.J., Xavier, J.C., 2018. Choosing the future of Antarctica. Nature 558 (7709), 233–241. https://doi.org/10.1038/s41586-018-0173-4.

Sokolov, S., Rintoul, S.R., 2009. Circumpolar structure and distribution opf the Antarctic circumpolar current fronts: 2. Variability and relationship to the surface height. J. Geoph. Res. 114 (C11), 15 pp. https://doi.org/10.1029/2008/C005248.

Tolman, H.L., 2002. Alleviating the garden sprinkler effect in wind wave models. Oc. Modelling 4 (3–4), 269–289. https://doi.org/10.1016/S1463-5003(02)00004-5.

Young, I.R., 1994. On the measurement of directional wave spectra. Appl. Ocean Res. 16 (5), 283–294. https://doi.org/10.1016/0141-1187(94)90017-5.

Young, S.H., 2016. A southeast Pacific basin subtropical cyclone off the Chilean coast. In: Blunden, J., Arndt, D. (Eds.), State of the Climate in 2015, Special Supplement to the Bulletin of the American Meteorological Society (BAMS) 97 (8), 129–130. https://doi.org/10.1175/2016BAMSStateoftheClimate.1.